



Featuring work from the Microfluidics Group of Prof. Claudio Berli at *Instituto de Desarrollo Tecnológico para la Industria Química (INTEC)* and the Optofluidics Laboratory of Prof. Raul Urteaga at *Instituto de Física del Litoral (IFIS-Litoral), Universidad Nacional del Litoral* and CONICET, Santa Fe, Argentina.

Title: Rational design of capillary-driven flows for paper-based microfluidics

A designing tool based on the solution of the inverse problem of capillary filling, which enables a precise programming of fluid transport in paper-like substrates and slit microchannels.

As featured in:



See Claudio L. A. Berli et al. *Lab Chip*, 2015, 15, 2173.



www.rsc.org/loc

Registered charity number: 207890



Cite this: *Lab Chip*, 2015, 15, 2173

Received 19th December 2014,
Accepted 13th March 2015

DOI: 10.1039/c4lc01487a

www.rsc.org/loc

Rational design of capillary-driven flows for paper-based microfluidics†

Emanuel Elizalde,^a Raúl Urteaga^a and Claudio L. A. Berli^{*b}

The design of paper-based assays that integrate passive pumping requires a precise programming of the fluid transport, which has to be encoded in the geometrical shape of the substrate. This requirement becomes critical in multiple-step processes, where fluid handling must be accurate and reproducible for each operation. The present work theoretically investigates the capillary imbibition in paper-like substrates to better understand fluid transport in terms of the macroscopic geometry of the flow domain. A fluid dynamic model was derived for homogeneous porous substrates with arbitrary cross-sectional shapes, which allows one to determine the cross-sectional profile required for a prescribed fluid velocity or mass transport rate. An extension of the model to slit microchannels is also demonstrated. Calculations were validated by experiments with prototypes fabricated in our lab. The proposed method constitutes a valuable tool for the rational design of paper-based assays.

Introduction

Paper-based microfluidic devices for diagnostics have gained much interest in the last few years because of a series of advantages associated with the material itself, such as low-cost, compatibility with most of chemical and biochemical reactions, and the possibility to transport fluids by capillary action. Detailed descriptions of paper attributes, device manufacturing techniques, and the increasing number of applications are found in the comprehensive reviews recently published.^{1–5}

Concerning fluid transport, the advantage of passive pumping however entails a challenging problem: the need to precisely modulate the flow according to the requirements of the unitary processes carried out on the chip.^{6,7} This aspect is particularly relevant as the flow rate cannot be further adjusted once the device is fabricated, except in more sophisticated systems.^{8,9} In fact, capillary driven flows are determined by two main factors, the physicochemical properties of the interfaces involved and the geometrical characteristics of the flow domain in both the micro scale, which locally defines the curvature of air–liquid interfaces, and the macro scale, which controls the overall flow rate through mass continuity. Therefore, for a given morphology, for example paper strips, different effects are investigated such as fiber source and size,¹⁰ paper type,¹¹ and the addition of chemicals to

induce flow delays.¹² On the other hand, for a given porous substrate, the effect of macroscopic geometry on filling dynamics is intensely studied. Paper sheets with different shapes have been proposed to pump fluids with a specific dynamics: circular,¹³ rectangular,¹⁴ trapezoidal,¹⁵ sector-shaped,¹⁶ and different combinations of them.^{14–17}

In most of the studies cited above, calculations to predict the instantaneous position of the meniscus in the substrate consider a geometrical shape designed beforehand. The procedure is also used in the analysis of capillary imbibition of porous materials other than paper,^{18,19} and it is a direct calculation from a mathematical point of view. In contrast, the inverse calculation consists of determining the (*a priori* unknown) shape that produces a specified fluid velocity as a function of time. This possibility has not been discussed in the literature yet, and it is the objective of the present work. Actually, the fundamentals of this approach have been reported in recent work addressed to open capillaries of a circular cross section.²⁰ Here the inverse calculation for paper-based microfluidics is described and validated by experiments. This knowledge enables a precise geometrical design for liquid handling, which is ultimately encoded in the paper shape. On the basis of these calculations, some basic rules are proposed for the rational manipulation of capillary-driven transport in paper-like substrates. An extension of the model to slit microchannels is also presented.

Theory

Macroscopic modelling

This section describes the fluid dynamic model proposed for the capillary imbibition of paper-like porous media. A

^a IFIS-Litoral (UNL-CONICET) Güemes 3450, 3000, Santa Fe, Argentina

^b INTEC (UNL-CONICET) Güemes 3450, 3000, Santa Fe, Argentina.

E-mail: cberli@santafe-conicet.gov.ar; Tel: 54 342 4559175

† Electronic supplementary information (ESI) available: See DOI: 10.1039/c4lc01487a

macroscopic approach is used, which is quite reasonable for the purposes of the present work. In fact, the model considers fluid displacements over distances much larger than the pore size, so that the local flow through the intricate pore space can be overlooked. The macroscopic flow is also assumed to be stationary and free of inertia, in agreement with the extremely low Reynolds numbers reached at the pore level. The system is kept in isothermal conditions. Gravity is neglected, which restricts this modeling to horizontally placed paper sheets. Under these conditions (Stokes regime), the continuum fields of fluid velocity and pressure satisfy the following equations,²¹

$$\nabla \cdot \mathbf{v} = 0, \quad (1)$$

$$\mathbf{v} = -\frac{k}{\mu} \nabla p, \quad (2)$$

where \mathbf{v} is the average fluid velocity, p is the average pressure, μ is the fluid viscosity, and k is the permeability of the porous substrate. Eqn (1) represents mass conservation for incompressible fluids that undergo neither evaporation nor condensation. Eqn (2) is the well-known linear force-flux relation for porous media, historically designated as Darcy's law. In this equation, the material property k should be in principle represented by a second rank tensor; here it is written as a scalar, which implies an isotropic medium.

In the model system considered (Fig. 1), capillary action drives the fluid in the x direction with an average velocity $v(x)$. The flow domain involves a cross-sectional area $A(x)$ that varies along the flow path. Eqn (1) imposes that the flow rate $Q = v(x)A(x)$ is instantly uniform, thus eqn (2) can be integrated from $x = 0$ (at time $t = 0$) to the average distance l (at time t) advanced by the liquid front,

$$p_0 - p_c = Q \frac{\mu}{k} \int_0^l \frac{dx}{A(x)}. \quad (3)$$

In this expression, p_0 is the pressure at $x = 0$, and $p_c = p_{\text{atm}} - 2\gamma \cos \theta / r_{\text{eff}}$ is the average capillary pressure at the fluid front (Laplace's equation), where r_{eff} stands for the effective pore radius, γ is the air-liquid surface tension, and θ is the

equilibrium contact angle made by the liquid with the solid.²² It is worth noting that, in eqn (3) and hereafter, k is treated as a constant, meaning that the porous substrate is assumed to be macroscopically homogeneous and rigid. The flow domain shown in Fig. 1 also includes a hydrodynamic load, which involves a generic flow resistance R_0 that satisfies,

$$p_{\text{atm}} - p_0 = QR_0. \quad (4)$$

By defining, $\Delta p = p_{\text{atm}} - p_c$ the equations above can be added up to obtain the following relationship,

$$v(l) = \frac{\Delta p}{A(l) \left[R_0 + \frac{\mu}{k} \int_0^l \frac{dx}{A(x)} \right]} \quad (5)$$

where $v(l)$ is the fluid front velocity and $A(l)$ is the corresponding cross-sectional area. Taking into account that $v(l) = dl/dt$, subsequent integration of eqn (5) yields an implicit expression for the meniscus position l versus time t

$$\frac{kR_0}{\mu} \int_0^l A(l') dl' + \int_0^l \left[A(l') \int_0^{l'} \frac{dx}{A(x)} \right] dl' = Dt, \quad (6)$$

where $D = k\Delta p/\mu$ is a sort of diffusive coefficient (units of $\text{m}^2 \text{s}^{-1}$) that characterizes the substrate-fluid system. Alternatively, eqn (6) predicts the time to fill a piece of paper with an arbitrary cross section $A(l)$ and length l .

It is important to point out here that Δp is deliberately considered as a constant, which implies that the capillary pressure does not vary during the imbibition. Consequently, eqn (6) is restricted to porous substrates where r_{eff} , γ , and θ are uniform along the flow domain. There is however an interesting corollary of this assumption: eqn (6) is entirely valid for the capillary filling of open microchannels where both the contact angle and the curvature of the air-liquid interface are constant during the imbibition. The flow system that satisfies these requirements is that of slit microchannels with constant height h , width $w(x)$, and $h \ll w(x)$ in the whole domain, where the ideal Hele-Shaw flow is attained. Also for this system, $p = p_{\text{atm}} - 2\gamma \cos \theta / h$ and $k = h^2/12$, hence $D = h\gamma \cos \theta / 6\mu$.

Direct calculation

Therefore, the kinematics of paper imbibition can be predicted from eqn (6), provided that the function $A(x)$ is known. The procedure has been used in previous studies to calculate the filling dynamics of porous substrates with different geometrical shapes.¹⁶⁻¹⁹ It should be observed that we are reporting here a general formulation of the problem, which comprises the fluid imbibition of homogeneous porous media whose cross-sectional shape $A(x)$ may vary in one, two or three dimensions, provided that the flow is unidirectional. In what follows we describe typical examples of each case, on

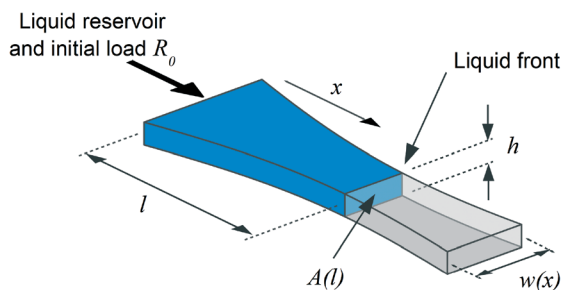


Fig. 1 Schematic drawing of the flow domain considered with the coordinate system used in calculations.

the basis of specifically shaped paper sheets, as shown schematically in Table 1.

The simplest situation corresponds to paper strips of uniform width and thickness. Solving eqn (6) with constants $A = A_0$ and $R_0 = 0$ leads to,

$$\frac{l^2}{2} = Dt, \quad (7)$$

which coincides with the well-known Lucas–Washburn (LW) dynamics for capillary tubes.^{23,24} Furthermore, the exact LW equation is obtained if one considers the most elemental microscopic model of the porous space: a bundle of parallel capillaries of radius r_{eff} aligned in the flow direction, for which $k = r_{\text{eff}}^2/8$, and hence $l^2 = (r_{\text{eff}}^2 \cos^2 \theta / 2\mu)t$. This result establishes a connection between the pore-scale geometry and the macroscopic representation used here.²⁵

Eqn (7) also serves as an asymptotic check for our modeling, since it is well documented that the imbibition kinematics of uniform paper strips obeys the $l \sim t^{1/2}$ relation, and is independent of strip width.^{10,14,17}

Next we consider a trapezoidal strip with a relatively small opening angle (Table 1). Solving eqn (6) with $A(x) = A_0(1 + ax)$ and $R_0 = 0$ leads to,

$$\frac{(1+al)^2}{2} \left[\ln(1+al) - \frac{1}{2} \right] + \frac{1}{4} = a^2 Dt, \quad (8)$$

where a is a parameter with units of m^{-1} . In the case of uniform thickness, a represents the tangent of the trapezoid angle normalized by the initial width w_0 . Notably, if one replaces $a = 1/r_0$ and $l = r - r_0$, the prediction of eqn (8) coincides with the radial imbibition of sector-shaped porous media,^{15,16} where r_0 is the radius of the wetted area at $t = 0$, as illustrated in Table 1. Indeed, this solution was firstly reported for the radial flow penetrating parallel disks from a small orifice of radius r_0 with infinite liquid supply.²⁶ The case corresponds to a flow domain with two-dimensional variation of $A(x)$ but still unidirectional flow.

Finally, an illustrative case of nonlinear variation of the cross-sectional area is $A(x) = A_0(1 + ax)^2$. After introducing this function and $R_0 = 0$ in eqn (6) one has,

$$\frac{1}{6} \left[(1+al)^3 - 1 \right] - \frac{1}{2} \left[(1+al)^2 - 1 \right] = a^2 Dt. \quad (9)$$

By analogy to the previous case, if one introduces $a = 1/r_0$ and $l = r - r_0$, eqn (9) coincides with the kinematics of radial imbibition into hemispherical porous media from a point source,¹⁸ where r_0 is the radius of the hemispherical wetted area at $t = 0$ (Table 1). In this case $A(x)$ presents a three-dimensional variation, however the flow is still unidirectional. For this geometry, the liquid front position evolves as $l \sim t^{1/3}$ at long times, where the limiting flow rate Q is nearly constant, in concordance with results for hemispherical porous media.¹⁸

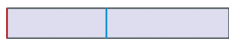
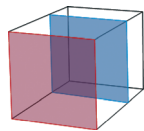
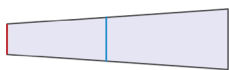
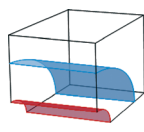
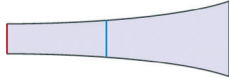
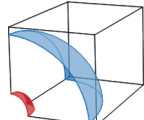
Inverse calculation

As stated in the Introduction, obtaining the velocity $v(x)$ or flow rate $Q(x)$ is designated as direct calculation, as eqn (6) can be straightforwardly solved for a given cross-sectional area $A(x)$. The objective of the present work is to discuss the inverse calculation: determining the unknown function $A(x)$ that produces a specified velocity $v(x)$ or flow rate $Q(x)$. For this purpose, eqn (5) is converted into a differential equation by using the Leibniz rule, and reordered to get an explicit expression of the cross-sectional profile $A(x)$ in terms of the desired flow rate function $Q(x)$,

$$A(x) = -\frac{Q(x)^2}{D} \left[\frac{dQ(x)}{dx} \right]^{-1}. \quad (10)$$

Thus eqn (10) predicts the shape $A(x)$ to be conferred to a piece of paper to attain a given flow rate $Q(x)$. Solving eqn (10) certainly helps to rationalize several engineering problems in paper-based microfluidics. For instance, the design

Table 1 Typical examples of paper imbibition kinematics predicted by the generalized model proposed here; eqn (6)

Cross-sectional area $A(x)$	Strip shape (top view)	Equation $l(t)$	Equivalent flow in porous media	Ref.	
A_0		(7)	1D (plane source)	Ref. 23,24	
$A_0(1 + ax)$		(8)	2D radial cylindrical (line source)	Ref. 26	
$A_0(1 + ax)^2$		(9)	3D radial spherical (point source)	Ref. 18	

of capillary pumps that provide a constant flow rate, which is largely explored at present;^{15,18,27} this particular case will be discussed later.

Here we move forward to include $Q(x) = v(x)A(x)$ into eqn (10). Thus, after calculations and reordering, one obtains the cross-sectional profile $A(x)$ in terms of the desired velocity function $v(x)$,

$$A(x) = \frac{v_0 A_0}{v(x)} \exp\left[-\frac{1}{D} \int_0^x v(x') dx'\right] \quad (11)$$

In this equation, $v_0 A_0 = \Delta p/R_0$ is the (initial) boundary condition. Here it is important to note that the hydrodynamic load R_0 cannot be disregarded in calculations, otherwise the area $A_0 = A(x=0)$ rests indeterminate, meaning that it could take multiple values, with an associated family of solutions that satisfies the velocity function $v(x)$.

For the purposes of illustration, here we solve the simple case of $v(x) = v_0$, which is however of practical interest, as it provides a new functionality in capillary imbibition: $l \sim t$. A paper sheet of uniform thickness h and variable width $w(x)$ is considered, as shown schematically in Fig. 2a. Further, the initial resistance is a portion of the same sheet with uniform width w_0 and length l_0 , so that $R_0 = \mu l_0/(khw_0)$ and $v_0 = \Delta p/(R_0 h w_0)$. Imposing this constant fluid velocity, eqn (11) is readily solved to give

$$w(x) = w_0 \exp\left(-\frac{x}{l_0}\right) \quad (12)$$

This remarkable simple result is illustrated in Fig. 2a. Furthermore, in view of applications, Fig. 2b and c include additional examples of geometrical forms that satisfy the requisite of constant fluid velocity: thick papers with out-of-plane

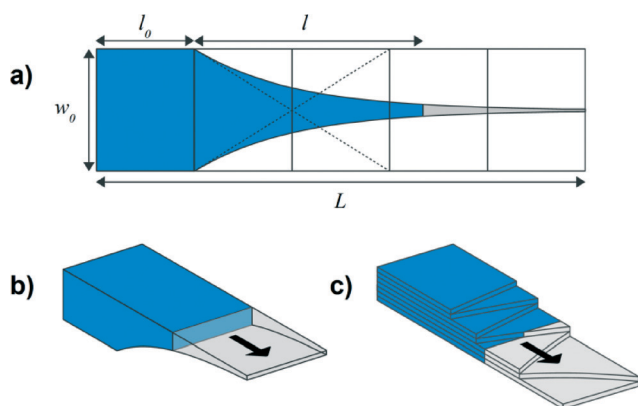


Fig. 2 Schematic representation of paper strips shaped to obtain constant fluid velocity according to eqn (12). (a) Paper sheet with uniform thickness, where the first section represents the hydrodynamic load and the second section has an exponentially decaying width. (b) Paper with uniform width and exponentially decaying thickness. (c) Multiple-folded sheet with uniform thickness and exponentially varying width.

exponential variation of the cross-sectional area and multiple-folded sheets with exponentially varying width. These formats would be more suitable for lateral flow assays and strip test.

Also concerning applications, it is worth noting that the initial flow resistance R_0 is a generic hydrodynamic load representing the region of the device where the required operations are performed. Naturally, this load antecedes the pumping section, and may have an arbitrary shape, provided that it is completely filled at the time our mathematical analysis begins. In contrast, the pumping section involves a specifically designed cross section, which is progressively filled with the liquid coming from the preceding zone.

Experimental systems reproducing the geometry of Fig. 2a were fabricated in our lab, in order to validate the prediction of eqn (12). Both paper sheets and slit microchannels were used for this purpose, as described below.

Materials and methods

Materials

Paper-based devices were made from Whatman qualitative filter paper (grade No. 1, 120 mm discs). Paper strips were shaped by using a drawing cutter with a thin blade. Highly hydrophobic double-sided adhesive tape (Stiko, Silkstone SA, Buenos Aires, Argentina) was used. Vinyl films 80 μm thick were used (McCall, Cat. 6031, McSign, New Taipei, Taiwan). Vinyl films were shaped with a cutting plotter (Moritzu UC-1350E). Borosilicate microscope slides 1 \times 3 inches were used (Sail Brand Cat. N $^\circ$ 7101). A hydro-soluble black colorant (STA stamp ink, Fapyc SA, Buenos Aires, Argentina) was employed to increase image contrast. Glycerol anhydrous and 2-propanol PA were provided by Laboratorios Cicarelli (Reagent SA, San Lorenzo, Argentina). Deionized water was produced by using an inverse osmosis purifier (Osmoion, Apema SRL, Villa Domingo Argentina).

Paper-based devices

Three layer systems were assembled as shown in Fig. 3a. The ensemble was mounted over a glass slide (not drawn) and covered with a second glass. The setup thus forms a rectangular microchannel laterally connected to a half-closed chamber that allocates paper strips. Liquid imbibition of several strips can be studied at the same time, under the same environmental conditions, and minimizing evaporation. Layer C is simply a double-sided hydrophobic tape to fix paper strips, prevent paper curling and confine the liquid movement into the paper strip. Layer B consists of paper strips and two tape spacers. Paper strip ends are partially inside the microchannel to make contact with the fluid. Layer A is also made from hydrophobic tape, and has several functions: on the back side of the scheme (Fig. 3a), the tape forms the microchannel walls and serves as a lateral barrier that avoids liquid creeping over the paper surface; on the front side of the scheme, it holds up the upper glass to maintain an air gap over paper strips. Before assembling the device, paper strips were shaped with a drawing cutter following specific blue

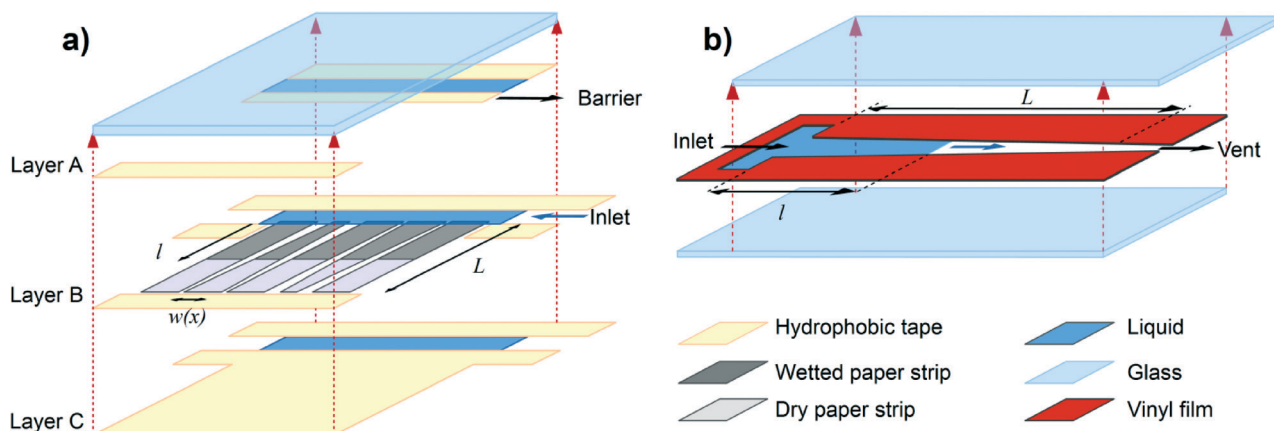


Fig. 3 3D exploded view of the fabricated chips (schematic representation). (a) Paper-based microfluidic device consisting of three layers of Whatman 1 filter paper and hydrophobic double-sided adhesive tape, sandwiched between two glass slides. The liquid is supplied through the rectangular microchannel formed on the back side (inlet), which enables the simultaneous imbibition of all the strips. (b) Hele-Shaw cell with constant height and variable width, fabricated by joining two microscope glass slides separated by a thin vinyl film. The liquid is supplied through the rectangular section transverse to the microchannel (inlet).

prints. Different patterns with the desired geometrical shapes were made by using CAD and then printed out. The initial strip width was always $w_0 = 1$ cm, and the total microchannel length was $L = 60$ mm.

Slit microchannels

Rectangular cross section microchannels with very small thickness in relation to the width were fabricated. The system consists of a shaped self-adhesive vinyl film (80 μm thickness) tightly fitted between two glass slides, as shown in Fig. 3b. The adhesive side of the film was placed in contact with the lower slide, according to the traditional transfer method used in the graphic market.²⁸ The ensemble was heated on a hot plate at 100°C for one minute. Then the upper glass slide was placed over the heated film and gently pressed to ensure the sealing of the microchannel borders. Before assembling the device, the vinyl film was shaped by using an electronic cutting machine, following a previously designed geometry. The initial width was always $w_0 = 5$ mm, and the smallest $w(x)$ reached was around 200 μm . The total microchannel length was $L = 60$ mm. The rectangular section on the left, transverse to the microchannel, forms the reservoir of the liquid that feeds the slit (inlet, Fig. 3b).

Experimental setup and measurements

Imbibition experiments were recorded by using a high resolution digital camera (Canon EOS 1000D). The microfluidic devices were placed horizontally over a white paper as a background. They were illuminated with an incandescent lamp. The irradiation was low enough to avoid a temperature increase over room temperature. The camera was focused vertically at a distance around 30 cm, connected to a PC, and set in burst mode. A stable frame rate was attained; EXIF image data were read to obtain the time vector. Experimental runs start when a small volume of liquid is poured into the inlet

microchannel. All the experiments were performed at room temperature. In paper-based devices, the liquid used was deionized water, with the addition of one drop of dye every 10 ml of water to increase the visual contrast; no chromatographic effect was observed. In slit microchannels, the chosen liquid was a 4:1 mixture of 2-propanol/glycerol. 2-Propanol has a low contact angle with both materials composing the microchannel walls (glass and vinyl film). Glycerol increases fluid viscosity and hence the temporal resolution of captured images. Black colorant was also added to improve visual contrast.

Image analysis

Fig. 4a and c show pictures of paper strips and slit microchannels, respectively, in typical imbibition experiments. A script was implemented to automatically analyze the images. The following steps were followed. The red channel of the RGB data for pictures was extracted to obtain a series of gray scale matrices $A(x, y; t)$. The area of interest in each picture was cropped to obtain a second series of gray scale matrices $B(x, y; t)$. In order to use the correct pixels only, the first image $B(x, y, t = 0)$ was subtracted from the last one $B(x, y, t = t_{\text{fill}})$. The results were converted into a 1 bit b/w mask $M(x, y)$. Using this mask and taking the mean grey value of each column of pixels in B , a gray scale profile for every instant $P(x, t)$ was obtained. Normalized profiles $P_n(x, t)$ were calculated after dividing by the last profile $P(x, t_{\text{fill}})$ (full wetted). Finally, the position l of the liquid front was obtained by searching the condition $P(l, t) = 0.15$. The resulting vectors $l(t)$ are those plotted in Fig. 4b and d.

Results and discussion

The fabricated prototypes were tested in capillary imbibition experiments, in order to validate the prediction of eqn (12).

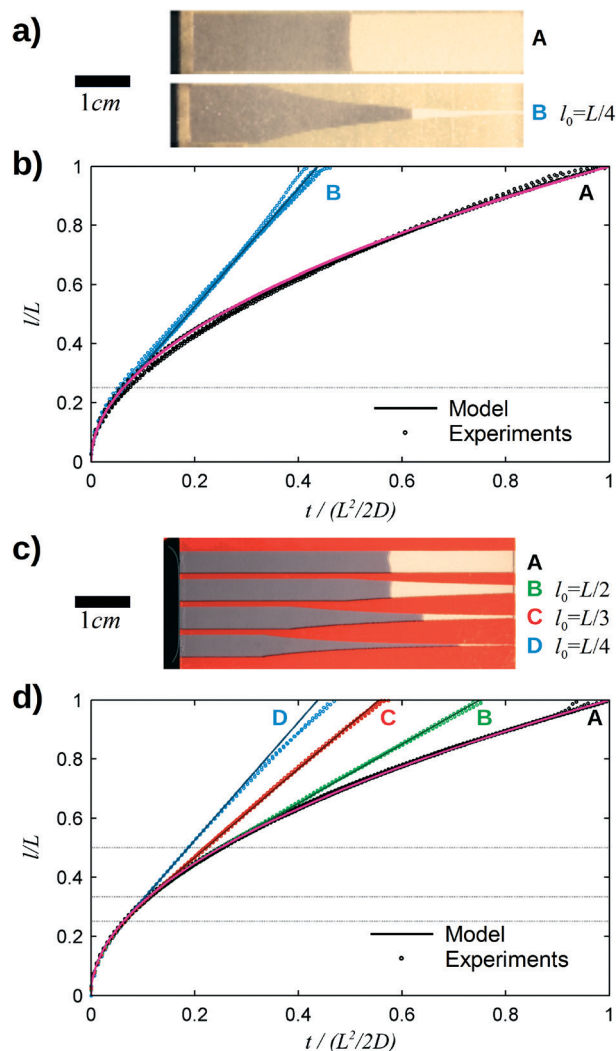


Fig. 4 Experimental results of fluid imbibition in both paper strips and slit microchannels. a) Photograph of the paper-based microfluidic device during imbibition. The image was taken at $t \sim 225$ s after water imbibitions started. Dark blue areas are wetted zones. Strips labelled A have constant width and were used as a reference. Strips labelled B have exponentially varying widths to produce constant fluid velocity at the advancing front, according to eqn (12). b) Experimental data (symbols) and model predictions (lines) of the liquid front position as a function of non-dimensional time for the strips shown in Fig. 4a. The horizontal dotted line indicates the position at which the exponential section begins. c) Photograph of slit microchannels during imbibition. The image was taken at $t \sim 35$ s after liquid imbibition started. Dark blue areas are filled zones. The slit labelled A has constant width. Slits labelled B, C, and D have exponentially varying widths, with initial loads of length $L/2$, $L/3$, and $L/4$, respectively. d) Experimental data (symbols) and model predictions (lines) of the liquid front position as a function of non-dimensional time for the slit microchannels shown in Fig. 4c. Horizontal dotted lines indicate the positions at which the exponential section begins.

Both paper sheets and slit microchannels were used for this purpose, as illustrated in Fig. 4. Systems of uniform width were also included as a reference, which must reproduce LW dynamics. Several experimental runs performed on similar devices are shown to illustrate the repeatability of the

imbibition dynamics. In Fig. 4b and d, data for the relative liquid front position l/L are presented as a function of non-dimensional time $t/(L^2/2D)$, where the value of diffusive coefficient was obtained from the best fit of the model to each experimental curve. Results were $D = 2.1 \pm 0.4 \text{ mm}^2 \text{ s}^{-1}$ for paper strips and $D = 18.6 \pm 0.6 \text{ mm}^2 \text{ s}^{-1}$ for slit microchannels. Thus the filling time of uniform paper strips was $L^2/2D \sim 900$ s, while that of slit microchannels with uniform width was around 96 s.

For paper strips with exponentially varying width, the example shown in Fig. 4a involves $l_0 = L/4$, which produces the filling dynamics reported in Fig. 4b. The linear time dependence of $l(t)$ starts precisely at the onset of the exponentially decaying width, as predicted by the model. For these experiments, the dispersion of D ($\sim 20\%$) is associated with the non-uniform microstructure of Whatman 1 filter paper (liquid properties can be assumed constant), presumably from heterogeneities in cellulose fiber orientation and compactness. Further research on this particular subject is of much interest, Whatman 1 being a popular substrate used in paper-based assays.¹¹

For experiments with slit microchannels (Fig. 4c and d), three different values of l_0 were used, namely $L/2$, $L/3$ and $L/4$. Again, the linear time dependence is observed along the region with an exponentially decaying cross section, precisely as predicted by the model. The total filling time is always lower than that of uniform slits of the same length, and it can be adjusted by modifying l_0 . It is worth noting that this variable, which also represents the initial hydrodynamic load R_0 , strongly influences the geometrical design of the device, as the initial fluid velocity obeys $v_0 = \Delta p/(R_0 A_0)$. This aspect is further considered later in relation to the flow rate Q .

In the case of the microchannel with the smallest value of l_0 , the front velocity slightly decreases at the end of the filling process (Fig. 4d). In this region, the microchannel width w is comparable to the height h , thus deviating from the Hele-Shaw flow conditions assumed in the model.³⁰ In addition, small systematic errors introduced in microfabrication become more significant in thin microchannels. In any case, the dispersion of the diffusive coefficient D ($\sim 3\%$) was much smaller than that obtained for paper strips.

Up to this point we have analyzed the design of paper-based devices for a desired fluid velocity $v(l)$, on the basis of eqn (11). In what follows we discuss the problems associated with the prescription of flow rates $Q(l)$, on the basis of eqn (10). The first aspect to be noted is that, in contrast to the case of $v(l) = Q(l)/A(l)$, flow rates $Q(l)$ are restricted to monotonically decreasing functions (for increasing $Q(l)$, eqn (10) would imply a non-physical negative area). In practice, it means that the hydrodynamic resistance $\Delta p/Q(l)$ always increases with l along the flow domain. Furthermore, constant flow rates can be reached only asymptotically, at very long times, as in the case of parabolic-shaped papers (Table 1) and hemispherical porous media¹⁸ (see also ref. 25 regarding the case of slit microchannels with varying cross sections). Actually eqn (10) enables constant Q values for a sudden expansion

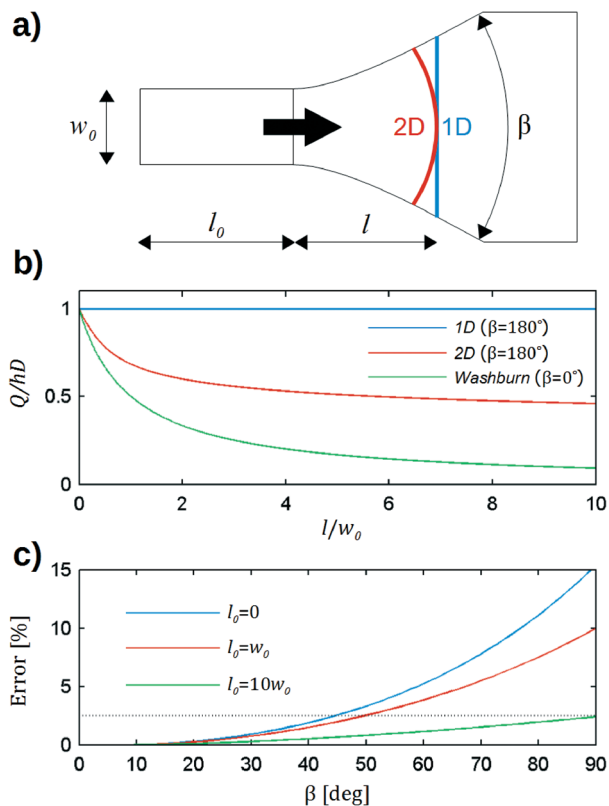


Fig. 5 a) Schematic drawing of fluid imbibition in a paper piece with a hyperbolic expansion in the direction of the flow. The region of uniform width w_0 and length l_0 represents a generalized initial load, and β denotes the opening angle of the expansion. In the hyperbolic section, the 2D model²⁹ predicts an elliptical liquid front (red curve) whereas the 1D model considered here involves a flat front (blue line). b) Non-dimensional flow rate Q/hD predicted by both models (1D blue curve; 2D red curve) as a function of non-dimensional distance for a sudden expansion ($\beta = 180^\circ$) with $l_0 = w_0$. Model prediction for a uniform strip falls onto the same curve (green). c) Relative error ($(Q_{1D} - Q_{2D})/Q_{2D}$) as a function of opening angle β for different initial loads. Error was calculated at $l = 10w_0$.

of the cross-sectional area, however the hypothesis of one-dimensional flow is no longer valid under these conditions.

Precisely, the limits of the model derived from the assumption on one-dimensional flow are revised next. For this purpose, we take as a reference the analytical solution of two-dimensional imbibition of porous media in flow domains that open with hyperbolic shape.²⁹ The geometry is schematically shown in Fig. 5a, where β is the opening angle of the expansion. For this specific shape, the two-dimensional model (ref. 29; see also ESI†) predicts an elliptical liquid front (red curve, Fig. 5a), whereas the one-dimensional model (present work, ESI) involves a flat liquid front (blue line, Fig. 5a). Flow rates obtained with each model are shown in Fig. 5b for $\beta \rightarrow 180^\circ$ (sudden expansion) and with $\beta \rightarrow 0^\circ$ (uniform width). In this last case, both models produce the same result, which coincides with the LW regime, as expected. The relative error of the one-dimensional model, $(Q_{1D} - Q_{2D})/Q_{2D}$, is presented in Fig. 5c as a function of the opening angle β , for different initial loads (calculations are

included in the ESI†). The one-dimensional model presents an error less than 2.5% for $\beta = 45^\circ$, for the extreme case $l_0 = 0$.

The above analysis leads to some corollaries of practical interest: independent of the model, the maximum flow rate to be attained is $Q_0 = \Delta P/R_0$, therefore it is defined by the initial load R_0 . Beyond this value, $Q(l)$ will always be a monotonically decreasing function, lying below the red curve in Fig. 5b. Within these limits, arbitrary $Q(l)$ functions can be experimentally attained by shaping expansions with the corresponding $A(l)$ profile predicted by eqn (10). In cases where wide opening angles are required, Fig. 5c helps one to check the error committed for a given initial load, and eventually redesign the prototype. Best results (minimum error in shape design) will be obtained for initial loads that are rather large in comparison with the resistance of the pumping section. Of course, near constant flow rates are more easily obtained in this limit as well.

Conclusions

Throughout this work we have theoretically analysed the capillary imbibition in paper-like substrates, paying particularly emphasis on the control of fluid kinematics by shaping the macroscopic geometry of the fluid domain. A fluid dynamic model was derived by assuming one-directional macroscopic flow in homogeneous porous substrates with arbitrary cross-sectional shapes. The novelty and the usefulness of this work are associated with the mathematical solution of the inverse problem, which allows one to determine the cross-sectional shape required for a prescribed fluid velocity or mass transport rate. Calculations were experimentally validated by using prototypes fabricated in our lab. For the sake of simplicity, the particular case of constant fluid velocity was used to prove the concept, but model predictions are in principle valid for any velocity function, under the restriction of monotonically decreasing flow rates.

Understanding the fundamentals of transport dynamics in paper-based assays certainly constitutes the basis for further developments in the field. In addition, concerning the applications itself, it is worthy to stress that designing lab-on-a-chip devices that integrate passive pumping requires a precise programming of the fluid dynamics, which has to be encoded in the geometrical shape of the substrate. This requirement becomes critical in processes with sequential steps, where the control over the time for each operation must be accurately accomplished,^{12,14} as well as in devices that take advantage of laminar capillary flow, such as the fuel cell on paper recently reported.³¹ In this sense, one may conclude that the model proposed constitutes a valuable tool to rationally design precise and reproducible paper-based assays.

Acknowledgements

The authors acknowledge the financial support received from the Consejo Nacional de Investigaciones Científicas y Técnicas (CONICET) and the Universidad Nacional del Litoral (UNL), Argentina.

References

- 1 X. Li, D. R. Ballerini and W. Shen, *Biomicrofluidics*, 2012, **6**, 011301.
- 2 A. K. Yetisen, M. S. Akram and C. R. Lowe, *Lab Chip*, 2013, **13**, 2210.
- 3 C. Parolo and A. Merkoçi, *Chem. Soc. Rev.*, 2013, **42**, 450.
- 4 W. K. T. Coltro, C.-M. Cheng, E. Carrilho and D. P. de Jesus, *Electrophoresis*, 2014, **35**, 2309.
- 5 C. R. Mace and R. N. Deraney, *Microfluid. Nanofluid.*, 2014, **16**, 801.
- 6 S.-J. Kim, S. Paczesny, S. Takayama and K. Kurabayashi, *Lab Chip*, 2013, **13**, 2091.
- 7 R. Safavieh and D. Juncker, *Lab Chip*, 2013, **13**, 4180.
- 8 C. K. W. Koo, F. He and S. R. Nugen, *Analyst*, 2013, **138**, 4998.
- 9 B. J. Toley, B. MacKenzie, T. Liang, J. R. Buser, P. Yager and E. Fu, *Anal. Chem.*, 2013, **85**, 11545.
- 10 A. Böhm, F. Carstens, C. Trieb, S. Schabel and M. Biesalski, *Microfluid. Nanofluid.*, 2014, **16**, 789.
- 11 E. Evans, E. F. M. Gabriel, W. K. T. Coltro and C. D. Garcia, *Analyst*, 2014, **139**, 2127.
- 12 B. Lutz, T. Liang, E. Fu, S. Ramachandran, P. Kauffmana and P. Yager, *Lab Chip*, 2013, **13**, 2840.
- 13 M. Conrath, N. Fries, M. Zhang and M. E. Dreyer, *Transp. Porous Media*, 2010, **84**, 109.
- 14 E. Fu, S. A. Ramsey, P. Kauffman, B. Lutz and P. Yager, *Microfluid. Nanofluid.*, 2011, **10**, 29.
- 15 S. Mendez, E. M. Fenton, G. R. Gallegos, D. N. Petsev, S. S. Sibbett, H. A. Stone, Y. Zhang and G. P. Lopez, *Langmuir*, 2010, **26**, 1380.
- 16 X. Wang, J. A. Hagen and I. Papautsky, *Biomicrofluidics*, 2013, **7**, 014107.
- 17 D. Shou, L. Ye, J. Fan, K. Fu, M. Mei, H. Wang and Q. Chen, *Langmuir*, 2014, **30**, 5448.
- 18 J. Xiao, H. A. Stone and D. Attinger, *Langmuir*, 2012, **28**, 4208.
- 19 Y. S. Joung, B. M. Figliuzzi and C. R. Buie, *J. Colloid Interface Sci.*, 2014, **423**, 143.
- 20 E. Elizalde, R. Urteaga, R. R. Koropecski and C. L. A. Berli, *Phys. Rev. Lett.*, 2014, **112**, 134502.
- 21 R. B. Bird, W. E. Stewart and E. N. Lightfoot, *Transport Phenomena*, John Wiley & Sons, New York, 1960.
- 22 P. G. de Gennes, F. Brochard-Wyart and D. Quéré, *Capillarity and Wetting Phenomena*, Springer-Verlag, New York, 2004.
- 23 R. Lucas, *Kolloid-Z.*, 1918, **23**, 15.
- 24 E. W. Washburn, *Phys. Rev.*, 1921, **17**, 273.
- 25 A. Marmur, *Langmuir*, 2003, **19**, 5956.
- 26 A. Marmur, *J. Colloid Interface Sci.*, 1988, **124**, 301.
- 27 W. van der Wijngaart, *Microfluid. Nanofluid.*, 2014, **16**, 829–837.
- 28 D. A. Bartholomeusz, R. W. Boulté and J. D. Andrade, *J. Microelectromech. Syst.*, 2005, **10**, 1364.
- 29 E. M. Benner and D. N. Petsev, *Phys. Rev. E: Stat., Nonlinear, Soft Matter Phys.*, 2013, **87**, 033008.
- 30 K. Petkovic-Duran and Y. Zhu, *Proc. SPIE 8204, Smart Nano-Micro Materials and Devices*, 2011, p. 82040M.
- 31 J. P. Esquivel, F. J. Del Campo, J. L. Gómez de la Fuente, S. Rojas and N. Sabaté, *Energy Environ. Sci.*, 2014, **7**, 1744.